# Space-coiling metamaterials with double negativity and conical dispersion

Zixian Liang[1], Tianhua Feng[1], Shukin Lok[1], Fu Liu[1], Kung Bo Ng[2], Chi Hou Chan[2], Jinjin Wang[3], Seunghoon Han[4], Sangyoon Lee[4], and Jensen Li[1,5]

[1]Department of Physics and Materials Science, City University of Hong Kong, Tat Chee Avenue, Kowloon Tong, Kowloon, Hong Kong, China.
[2]State Key Laboratory of Millimeter Waves, City University of Hong Kong, Tat Chee Avenue, Kowloon, Hong Kong, China.
[3]Kuang-Chi Institute of Advanced Technology, Shen Zhen, Guangdong, China.
[4]Samsung Advanced Institute of Technology, Samsung Electronics, South Korea.
[5]School of Physics and Astronomy, University of Birmingham, Birmingham B15 2TT, UK.
email: j.li@bham.ac.uk

**Supplementary Figures**

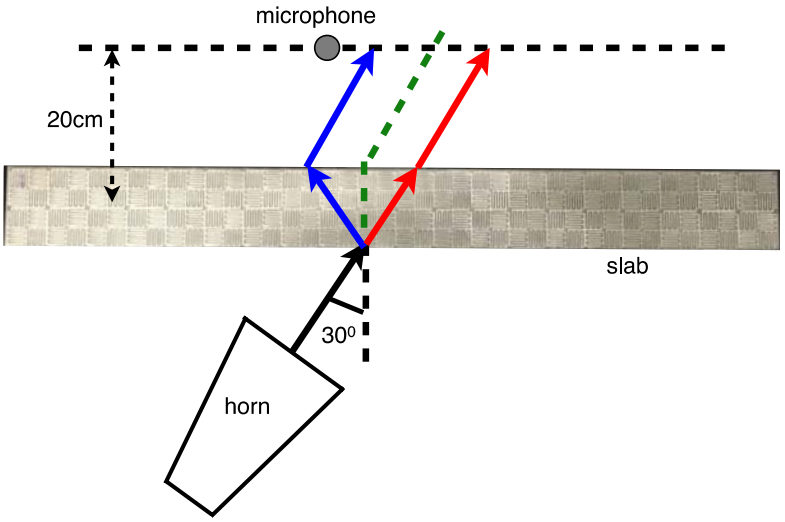


**Figure S1. Schematic of the 2D pressure-profile measurement for demonstrating positive or negative refraction using the space-coiling metamaterials.** Negative refraction (blue arrow representing the path of ray) and positive refraction (red arrow representing the path of ray) of the slab constructed with 2x20 units. The green dashed line differentiates negative and positive refraction. A horn embedded in the system shines a beam with width 20cm at an incidence angle of 30 degrees to the slab. A microphone is inserted in the waveguide and scans the pressure field profile at a distance

of 20 cm to the center of the slab. The microphone is moved in step of 2cm, in a subwavelength resolution in our frequency region, in the scanning to obtain a smooth beam profile in space.

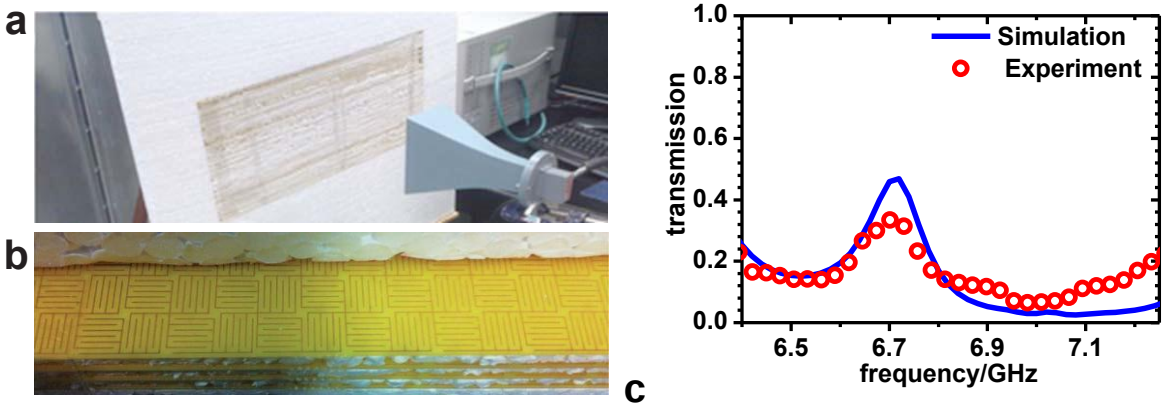


**Figure S2. Experimental setup of electromagnetic wave measurement. a.** Side view of setup of the measurement system. Two horn antennas on both sides of the sample measures the S-parameters and the beam shift (profile) with a network analyzer. **b.** A closer view of the sample. It composes of stratified layers of the copper wires of the same pattern printed on PCBs, separated by foam spacers of subwavelength thickness. H-fields from the horns is directed perpendicular to the copper-wire layers. **c.** The simulation (blue line) and experimental (red circles) transmission of the sample at normal incidence.

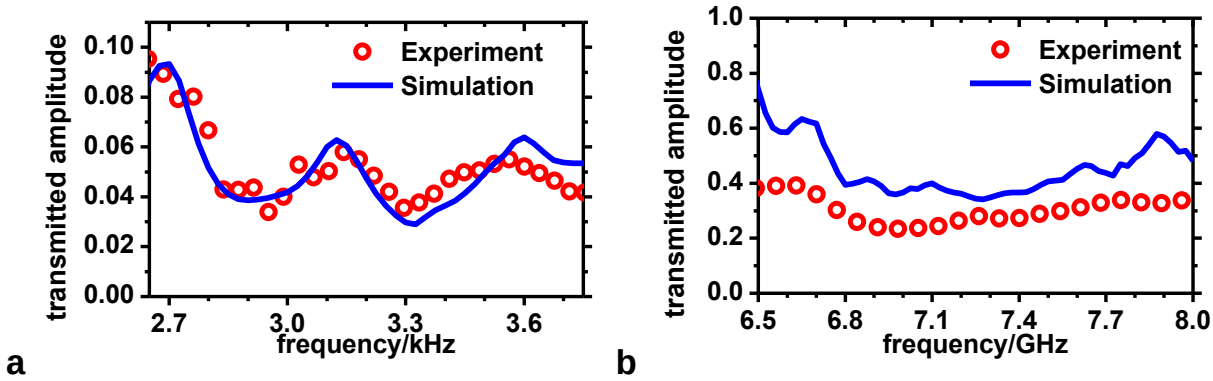


**Figure S3. Transmitted amplitude of the slabs with incident beam at 30 degrees. a.** Acoustic slab, **b.** Electromagnetic slab. Blue lines: simulation results, red circles: experimental results. For acoustic

slab, the drop in amplitude is contributed by absorption loss due to viscosity, and reflection due to impedance mismatch from air to metamaterial and also an additional impedance mismatch from the difference in height of measurement waveguide (2.6cm) and channel height (1cm) in a practical sample. For electromagnetic slab, the drop is due to absorption loss in FR-4 (dielectric substrate of PCB), impedance mismatch from air to sample and the additional scattering loss due to the open space environment in experiment. Also, the slight dislocation between different PCB layers may also introduce the loss.

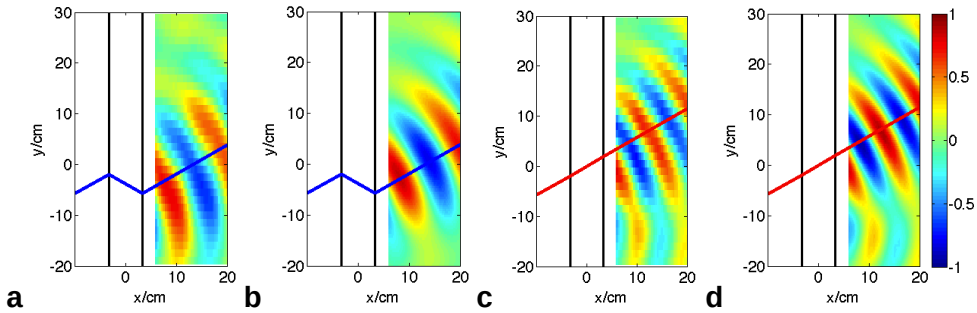


**Figure S4 Pressure profile after the acoustic metamaterial slab with incident beam at 30 degrees.** Results of experiement **a** $n \approx -1$ at 2.7kHz and **c** $n \approx 1$ at 3.7kHz, and **b** and **d** are the corresponding simulation results. The black solid lines represent the slab surface. The blue lines represent the negative refraction path, and the red one represent the positive refraction path.

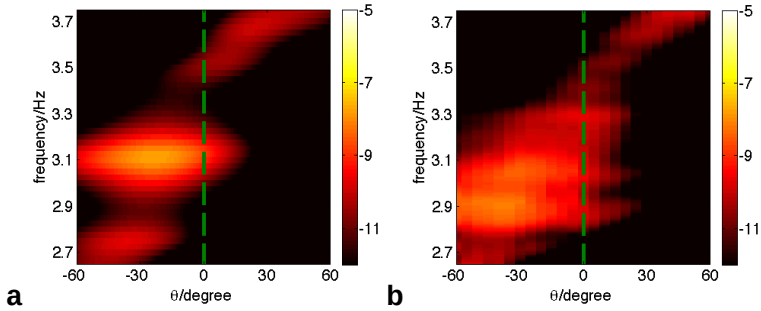


**Figure S5. Pressure amplitude profile (in dB) for an acoustic beam shining on the metamaterial prism with 45 degrees inclination. a.** Simulation results, and **b.** experimental results. The amplitude

drop is due to similar reasons as explained in Fig. S3. If we normalized to its maximum value to show the exit beam direction at each frequency, the results are showed as Fig. 4 in text.

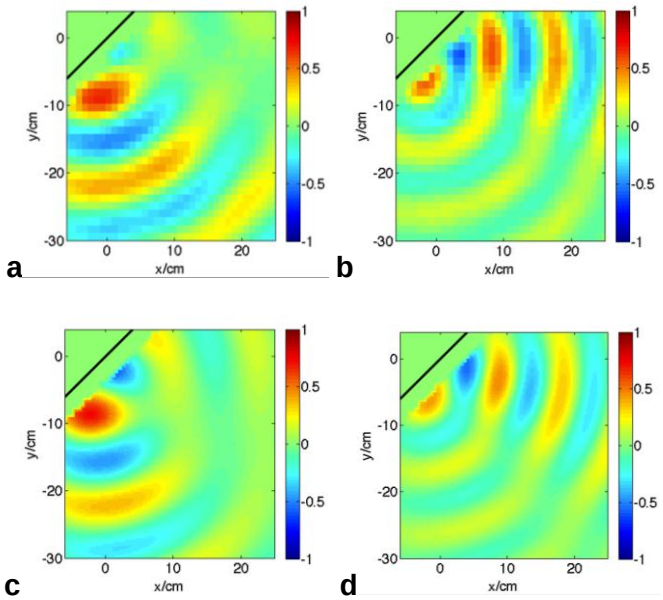


**Figure S6 Pressure profile after prism in 2D. The incident beam is shined to the prism along x-direction**. Results of experiement **a** $n \approx -1$ for negative refraction at 2.7kHz and **b** $n \approx 1$ for positive refraction at 3.7kHz, and **c** and **d** are the corresponding simulation results respectively. The black lines represent the prism surface.

## Supplementary Methods

### 1) Direct acoustic attenuation measurement

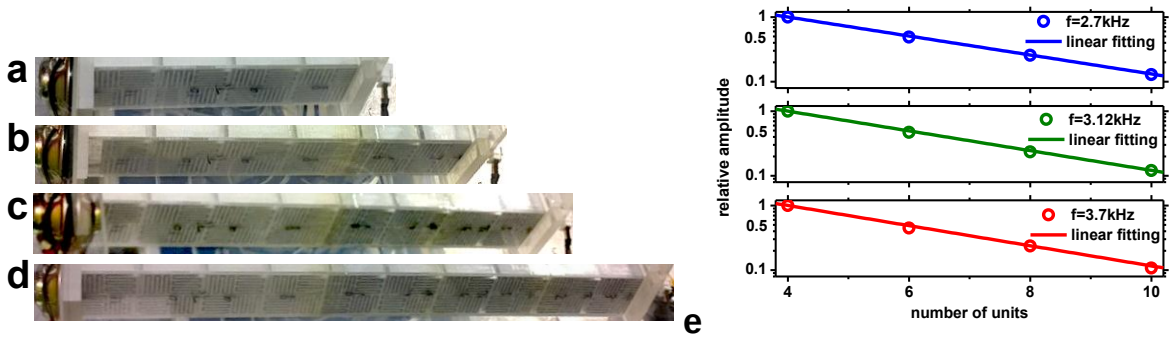


**Figure S7. The acoustic attenuation measurement. a-d.** Acoustic space-coiling metamaterials array with 4x1, 6x1, 8x1, and 10x1 units. A speaker fires pulses from left side of the array and a

microphone measures the transmitted signal at the right side. **e.** The signal amplitude of different units at 2.7kHz, 3.12kHz, and 3.7kHz.

By directly measuring the transmission of samples with varying length in the wave propagating direction within a waveguide, we can obtain the attenuation of the acoustic coiling metamaterial against frequency. We measured the transmitted signals for the units of different array sizes. A pulse is fired to each array of 4x1, 6x1, 8x1, and 10x1, shown in Fig. S7. For each measurement, only the primary pulse signal arriving the detector is collected (without the multiple reflected signal within the sample) and the signal amplitude exponentially decays with the increase of the number of units. Then, by applying Fourier transform, the attenuation and hence the Im(n) spectrum are obtained.

**2) Absorption loss of the acoustic coiling metamaterial from viscosity and thermal conduction**

Our approach of phase delay by space coiling for extreme indices does not rely on the local resonance of the metamaterials units, so there is no resonant absorption associated to the local resonance. The loss of the coiling metamaterials mainly comes from the viscosity and accumulates in propagation in channel.

We defined an intensity attenuation coefficient $\alpha$ for a channel filled with air, which includes the intensity attenuation from two contributions being labeled by viscosity $\alpha_{\omega\eta}$ and thermal conduction $\alpha_{\omega\kappa}$. Following Ref. 40, in a straight channel with rectangular cross-section with width *w* and height *h*, the attenuation coefficient can be obtained by

$$\alpha = \alpha_{\omega\eta} + \alpha_{\omega\kappa},\ \alpha_{\omega\eta} = \frac{w+h}{wh}\frac{1}{c}\sqrt{\frac{4\pi\eta f}{\rho_0}},\ \alpha_{\omega\kappa} = \frac{\gamma-1}{\sqrt{\mathrm{Pr}}}\alpha_{\omega\eta}, \tag{S1}$$

where $c$ = 343m/s is the sound speed in air, $\rho_0 = 1.21 kg/m^3$ is the density of air, $\mathrm{Pr} = 0.71$ is the Prandtl number, $\gamma = 1.402$ is the ratio of specific heats, $\eta = 1.85\times10^{-5} Pa\bullet s$ is the dynamic viscosity for air, and $f$ is

the frequency of the wave propagating in the channel. Then $\alpha = \frac{w+h}{wh}\xi\sqrt{f}$ is obtained, where $\xi = (1+\frac{\gamma-1}{\sqrt{\Pr}})\frac{1}{c}\sqrt{\frac{4\pi\eta}{\rho_0}} = 5.97\times10^{-5}s^{1/2}$. Therefore, there will be an additional imaginary part to the refractive index of air in each channel, which can be effectively defined as $\mathrm{Im}(n) = \frac{\alpha}{2k_0}$. This value is incorporated in the refractive index of air within the curled channels in all the acoustic simulations with microstructures.

**3) Tunable ratio between wavelength and size of unit cell**

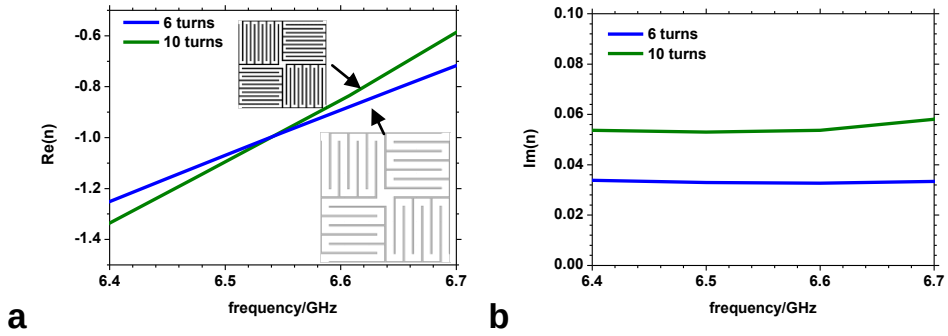


**Figure S8. Refractive index of EM space-coiling metamaterial for different number of turns.** The effective refractive index (*n*) **a** real part and **b** imaginary part of space-coiling metamaterial with 6 turns (blue line) /10 turns (green line) with lattice constant *a* of 0.76/0.56cm obtained from simulations. Index n=-1 is fixed at 6.54GHz for both structures. The two insets show the two structures with different number of turns from corner to center of the unit. Black/white color represents the copper wires/channels.

Our geometric route of coiling up space has the advantage that the ratio between wavelength and unit cell size $\lambda / a$ can be easily changed by varying the number of turns. For example, we can make 10 turns (4 additional turns are added, comparing to the structure in text) in the curled channels from each corner to center in the unit (shown in the insets of Fig. S8). The unit cell size is scaled down from 0.76 to 0.56cm to keep the same

working frequency in the microwave regime (channel/metal wires width is 0.46mm/0.11mm, the spacer thickness is 1.7mm and the periodicity of the layers is 2mm). The simulated effective index is found as n=-1 at 6.54GHz for both cases shown in Fig. S8. It changes $\lambda / a$ for that frequency from 6 to 8.1, with a 35% increase.